Solute molecular dynamics in a mesoscale solvent

Cite as: J. Chem. Phys. **112**, 7260 (2000); https://doi.org/10.1063/1.481289
Submitted: 16 July 1999 . Accepted: 03 February 2000 . Published Online: 12 April 2000

Anatoly Malevanets, and Raymond Kapral

Solute molecular dynamics in a mesoscale solvent

Anatoly Malevanets[a)]
Department of Physics, Theoretical Physics, Oxford University, 1 Keble Road, Oxford OX1 3NP, United Kingdom

Raymond Kapral
Chemical Physics Theory Group, Department of Chemistry, University of Toronto, Toronto M5S 3H6, Canada

(Received 16 July 1999; accepted 3 February 2000)

A hybrid molecular dynamics (MD) algorithm which combines a full MD description of solute–solute and solute–solvent interactions with a mesoscale treatment of solvent-solvent interactions is developed. The solvent dynamics is modeled on a mesoscale level by coarse graining the system into cells and updating the velocities of the solvent molecules by multiparticle collisions within each cell. The solvent dynamics is such that the correct hydrodynamic equations are obtained in the macroscopic limit and a Boltzmann distribution of velocities is established in equilibrium. Discrete-time versions of the hydrodynamic equations and Green–Kubo autocorrelation functions are derived. Between the discrete-time solvent–solvent collisions the system evolves by the classical equations of motion. The hybrid MD scheme is illustrated by an application to the Brownian motion of a nanocolloidal particle in the mesoscale solvent and concentrated nanocolloidal suspensions. © *2000 American Institute of Physics.* [S0021-9606(00)50816-2]

I. INTRODUCTION

When studying complex fluids it is often convenient to focus on the dynamics of a subsystem of interest and treat the remainder of the system at a less detailed level of description. For instance, in colloidal suspensions one is interested in the dynamics of the colloidal particles, while the details of the solvent dynamics that influences their motions are of less interest. The classical theories of Brownian motion recognized this distinction and reduced the influence of the solvent on the Brownian particles to frictional forces and random forces with simple statistical properties.[1] In many applications such a simplified description does not suffice since one would like to account for specific features of the solute–solvent forces. In aqueous solutions, for example, these forces may be hydrophobic or hydrophilic and influence the dynamics of the solute molecules in rather different ways.

In this article we show how to combine a full molecular dynamics (MD) description of the solute motions, including the specific nature of their interactions with the solvent, with a mesoscale treatment of the solvent dynamics. The solvent model was introduced earlier[2] and consists of ''particles'' whose positions and velocities are treated as continuous variables. The system is coarse grained into cells, with no restriction on the number of particles that may reside in a cell, and the solvent dynamics is carried out synchronously at discrete time steps. Particle streaming is treated exactly while the cells are the collision volumes for a multiparticle collision dynamics. Since the solvent is treated as a collection of particles, collisional coupling to other microscopic solute degrees of freedom is easily taken into account.

a)Electronic mail: a.malevanets1@physics.ox.ac.uk

The features of this hybrid molecular dynamics are explored in this paper, which is organized as follows. In Sec. II we sketch the properties of the mesoscale solvent model and show how it can be combined with a full MD description of the solute dynamics. In order to study the influence of the solvent dynamics on solute motions it is necessary to analyze the pure solvent in some detail. Since the solvent dynamics is carried out at discrete time steps this necessitates a reexamination of standard correlation function treatments. In Sec. III the derivations of linearized hydrodynamic equations and Green–Kubo formulas for discrete time autocorrelation functions are given. In Sec. IV we illustrate the hybrid MD method by investigating the dynamics of a single solute nanocolloidal particle and a concentrated suspension of nanocolloidal particles in the mesoscale solvent. Section V contains the conclusions of the study.

II. HYBRID MOLECULAR DYNAMICS MODEL

We consider a system composed of a bath of N solvent molecules with phase space coordinates, $\mathbf{X}^{(N)} = (\mathbf{x}_1, \mathbf{x}_2, \ldots, \mathbf{x}_N)$ and $= \mathbf{V}^{(N)} = (\mathbf{v}_1, \mathbf{v}_2, \ldots, \mathbf{v}_N)$ and M solute molecules with phase space coordinates $\mathbf{X}^{(M)} = (\mathbf{x}_{N+1}, \mathbf{x}_{N+2}, \ldots, \mathbf{x}_{N+M})$ and $= (\mathbf{v}_{N+1}, \mathbf{v}_{N+2}, \ldots, \mathbf{v}_{N+M})$. The solute molecules interact with each other through an interaction potential $V_{\rm ss}(\mathbf{X}^{(M)})$ and with the solvent molecules through a potential $V_{\rm sb}(\mathbf{X}^{(M)}, \mathbf{X}^{(N)})$. The solvent–solvent potential energy is zero and the total potential energy is the sum of solute–solute and solute–solvent contributions, $V(\mathbf{X}^{(M)}, \mathbf{X}^{(N)}) = V_{\rm ss}(\mathbf{X}^{(M)}) + V_{\rm sb}(\mathbf{X}^{(M)}, \mathbf{X}^{(N)})$.

Time is partitioned into segments of length τ and the system is coarse grained into Wigner–Seitz cells. Within each such time interval τ all solute and solvent particles in the entire system evolve by Newton's equations of motion,

$$\dot{\mathbf{x}}_i = \mathbf{v}_i, \quad m_i \dot{\mathbf{v}}_i = -\frac{\partial V}{\partial \mathbf{x}_i} = \mathbf{F}_i, \tag{1}$$

where m_i is the mass of particle i. Because of the nature of the potential, within the time interval τ there are no solvent–solvent interactions.

The interactions between solvent particles occur at each discrete time step τ and take the form of multiparticle collisions among solvent molecules in each coarse-grained cell. In a collision event, the velocities of all particles in a frame moving with the velocity of the center of mass of the particles in a cell are rotated in a randomly chosen direction. These collision events are carried out independently in each cell. Thus, the multiparticle collisions transform the *solvent* particle velocities according to

$$\mathbf{v}_i \to \mathsf{V} + \hat{\omega}[\mathbf{v}_i - \mathsf{V}], \tag{2}$$

where $\hat{\omega}$ is a random rotation from a set Ω and V is the average velocity of the colliding particles within a cell. The mesoscale solvent dynamics is a type of direct simulation Monte Carlo[3] with a modified collision rule. During collisions the momentum and energy are conserved in each cell. The phase space volume during the transformation is preserved and the collision rule ensures that an equilibrium microcanonical ensemble distribution of the hybrid MD evolution exists.

This constitutes the hybrid MD model for the dynamics of the system. Since the solute particles interact with the solvent particles through intermolecular forces, solute–solute and solute–solvent interactions are treated microscopically, a feature which is crucial in many applications. However, since the solvent–solvent dynamics is treated in a mesoscale fashion through multiparticle collisions which act only at discrete time intervals, the evolution is efficient and large numbers of solvent molecules can be considered.

We have shown that the mesoscale solvent model correctly describes the hydrodynamics of the velocity field.[2] In the present applications, where one is interested in the solute molecule motions, it is first necessary to investigate the solvent–solvent correlation functions since these quantities enter directly into theoretical descriptions of solute dynamics. In view of the discrete nature of the solvent dynamics and the multiparticle collision rule a reexamination of the calculation of these correlation functions is required. Consequently, we first discuss the solvent correlations and then return to the solute correlations using the hybrid molecular dynamics scheme.

III. GREEN–KUBO FORMULAS FOR SOLVENT DYNAMICS

In this section we derive Green–Kubo formulas for discrete systems[4] in order to determine the time correlations and transport properties of the pure mesoscale solvent with no solute molecules present. In the following section we shall use these results to analyze solute Brownian motion in the solvent.

The starting point of the analysis is the evolution equation for phase space probability density of the multiparticle-collision model,[2]

$$P(\mathbf{V}^{(N)}, \mathbf{X}^{(N)} + \mathbf{V}^{(N)}, t+1) = \mathcal{C}P(\mathbf{V}^{(N)}, \mathbf{X}^{(N)}, t), \tag{3}$$

where the collision operator $\mathcal{C}$ has the form,

$$\mathcal{C}P(\mathbf{V}^{(N)}, \mathbf{X}^{(N)}, t) = \frac{1}{\|\Omega\|^L} \sum_{\Omega^L} \int d\check{\mathbf{V}}^{(N)} P(\check{\mathbf{V}}^{(N)}, \mathbf{X}^{(N)}, t) \times \prod_{i=1}^{N} \delta(\mathbf{v}_i - \mathsf{V}_{\boldsymbol{\xi}} - \hat{\omega}_{\boldsymbol{\xi}}[\check{\mathbf{v}}_i - \mathsf{V}_{\boldsymbol{\xi}}]). \tag{4}$$

Here $\check{\mathbf{V}}^{(N)} = (\check{\mathbf{v}}_1, \check{\mathbf{v}}_2, \ldots, \check{\mathbf{v}}_N)$ denotes the set of precollision velocities and $\boldsymbol{\xi}$ is the coordinate of a coarse-grained cell of the system. Letting $\Gamma = (\mathbf{V}^{(N)}, \mathbf{X}^{(N)})$ be a solvent phase point and $\mathcal{W}(\Gamma' \to \Gamma)$ the transition operator that accounts for the streaming and collision steps, we may write the discrete-time evolution equation formally as

$$\mathsf{P}(\Gamma, t+1) = \int d\Gamma' \mathcal{W}(\Gamma' \to \Gamma) \mathsf{P}(\Gamma', t), \tag{5}$$

where the integral sign implies summation over any discrete variables in the state Γ. The equilibrium distribution of this Markov chain is denoted by $P_0(\Gamma)$.

We shall derive a set of evolution equations for the locally conserved variables, mass, momentum and energy, using projection operator methods and extract discrete-time correlation function expressions for transport coefficients. The projection operator method we use follows the lines of the well-known reduction of the classical evolution of a Hamiltonian system to a generalized Langevin equation[5,6] but is modified to account for the intrinsic stochasticity and discrete-time dynamics of the model.

We define a projection operator $\mathcal{P}$ as

$$(\mathcal{P}H)(\Gamma) = H_{\mathcal{P}}(\Gamma) = \mathbf{a}^{\dagger}(\Gamma) P_0(\Gamma) \langle \mathbf{a}\mathbf{a}^{\dagger} \rangle^{-1} \times \int d\Gamma' \mathbf{a}(\Gamma') H(\Gamma'), \tag{6}$$

where $\mathbf{a}$ is a set of dynamical variables, $H(\Gamma)$ is any function of the phase space variables and the angular brackets denote an average over the equilibrium distribution. The complementary operator $\mathcal{Q}$ is defined by $\mathcal{Q} = 1 - \mathcal{P}$. Often we shall drop the argument Γ when ambiguity is unlikely to arise.

Consider the Fourier transform of a locally conserved dynamical variable defined as

$$a_{\mathbf{k}}(\Gamma(t)) = \sum_i \iota_i(t) e^{i\mathbf{k}\cdot\mathbf{x}_i(t)}.$$

Here $\iota(t)$ represents one of the collision invariants, mass, momentum, or energy, and $a_{\mathbf{k}}(\Gamma(t))$ is the corresponding density. Our main interest is in the small $\mathbf{k}$ dependence of these locally conserved dynamical variables. Application of the projection operator and it complement to Eq. (5) (the derivation is outlined in Appendix A) leads to

$$\mathsf{P}_{\mathcal{P}}(t+1) = \mathcal{P}\mathcal{W}\mathsf{P}_{\mathcal{P}}(t) + \sum_{\tau=1}^{t} \mathcal{K}(\tau - 1) \mathsf{P}_{\mathcal{P}}(t - \tau). \tag{7}$$

For locally conserved dynamical variables the memory kernel in this equation is given by

$$\mathcal{K}(\tau) = \mathcal{P}(\mathcal{W} - 1)\mathcal{Q}\mathcal{W}^{\tau}\mathcal{Q}(\mathcal{W} - 1)\mathcal{P} + o(\mathbf{k}^2). \tag{8}$$

A. Evolution of locally conserved variables

The average of the set of conserved quantities **a** over the projected probability distribution yields a set of equations for their average values $\overline{\mathbf{a}}(t)$. The derivation of this set of equations, starting from Eq. (7), is presented in Appendix B and the result in vector form is

$$\overline{\mathbf{a}}_t=\frac{1}{2}\langle \mathbf{a}(\mathcal{S}(\Gamma,1))\mathbf{a}^\dagger(\Gamma)-\mathbf{a}(\Gamma)\mathbf{a}^\dagger(\mathcal{S}(\Gamma,1))\rangle\langle \mathbf{a}\mathbf{a}^\dagger\rangle^{-1}\overline{\mathbf{a}} - \left[\frac{1}{2}\langle \mathbf{f}(0)\mathbf{f}^\dagger(0)\rangle+\sum_{t=1}^{\infty}\langle \mathbf{f}(t)\mathbf{f}^\dagger(0)\rangle\right]\langle \mathbf{a}\mathbf{a}^\dagger\rangle^{-1}\overline{\mathbf{a}}. \tag{9}$$

In Eq. (9) we have introduced an operator $\mathcal{S}(\Gamma,t)$ which relates to the state Γ at the initial time the set of states after t steps of evolution, weighted with the probability of transition to the corresponding state. Using this notation we may express equilibrium averages in the following form:

$$\int d\Gamma\int d\Gamma' a(\Gamma)\mathcal{W}(\Gamma'\to\Gamma)b(\Gamma')P_0(\Gamma') =\langle a(\mathcal{S}(\Gamma,1))b(\Gamma)\rangle,$$

where summation over states is implied. The quantity **f** in Eq. (9) is a random force defined by

$$\mathbf{f}(t)=\mathbf{a}(\mathcal{S}(\Gamma,t+1))-\langle \mathbf{a}(\mathcal{S}(\Gamma',1))\mathbf{a}^\dagger(\Gamma')\rangle \times\langle \mathbf{a}\mathbf{a}^\dagger\rangle^{-1}\mathbf{a}(\mathcal{S}(\Gamma,t)). \tag{10}$$

In Eq. (9) one finds the sum of the force–force time correlation function and this corresponds to a trapezoid approximation of the time integral found in derivations for continuous-time systems. We will use the following alternative expression for the sum of the force–force time-correlation function:

$$\frac{1}{2}\langle \mathbf{f}(0)\mathbf{f}^\dagger(0)\rangle+\sum_{t=1}^{\infty}\langle \mathbf{f}(t)\mathbf{f}^\dagger(0)\rangle=\lim_{\mathsf{T}\to\infty}\frac{1}{2\mathsf{T}}\sum_{t,t'<\mathsf{T}}\langle \mathbf{f}(t)\mathbf{f}^\dagger(t')\rangle. \tag{11}$$

B. Linearized hydrodynamic equations

Application of Eq. (9) to a complete set of conserved quantities leads to the linearized hydrodynamic equations. The system is partitioned into Wigner–Seitz cells with coordinates $\boldsymbol{\xi}$ as noted in Sec. II. The momentum and energy densities in a cell plus the particle density constitute the set of locally conserved variables:

$$\rho(\mathbf{x})=\sum_{i=1}^{N}\delta(\mathbf{x}_i-\mathbf{x}), \tag{12}$$

$$\boldsymbol{\mu}(\boldsymbol{\xi})=\sum_{i=1}^{N}\mathbf{v}_i\theta(1/2-|\mathbf{x}_i-\boldsymbol{\xi}|), \tag{13}$$

$$\varepsilon(\boldsymbol{\xi})=\sum_{i=1}^{N}\frac{1}{2}v_i^2\theta(1/2-|\mathbf{x}_i-\boldsymbol{\xi}|). \tag{14}$$

It is convenient to work with an orthogonal set of dynamical variables. In k space, where $\mathbf{k}$ is restricted by $|\mathbf{k}|<1/\pi$, the set of orthogonal dynamical variables is

$$\mathbf{a}_\mathbf{k}=\{\rho_\mathbf{k},\boldsymbol{\mu}_\mathbf{k},s_\mathbf{k}\},$$

where we introduced the notation $s_\mathbf{k}=\epsilon_\mathbf{k}-C_vT\rho_\mathbf{k}$ with C_v the specific heat. For this set of variables the cross-correlation matrix is indeed diagonal and has the following form:

$$\langle \mathbf{a}_\mathbf{k}\mathbf{a}_\mathbf{k}^\dagger\rangle=N\begin{pmatrix}1 & \mathbf{0} & 0\\ \mathbf{0} & k_BT\mathbf{1} & \mathbf{0}\\ 0 & \mathbf{0} & C_vk_BT^2\end{pmatrix}, \tag{15}$$

where $C_v=3k_B/2$ in three dimensions. The dissipation-free evolution is determined by the first term in Eq. (9) and one has

$$\tfrac{1}{2}\langle \mathbf{a}_\mathbf{k}(\mathcal{S}(\Gamma,1))\mathbf{a}_\mathbf{k}^\dagger(\Gamma)-\mathbf{a}_\mathbf{k}(\Gamma)\mathbf{a}_\mathbf{k}^\dagger(\mathcal{S}(\Gamma,1))\rangle =N\begin{pmatrix}0 & i\mathbf{k}k_BT & 0\\ i\mathbf{k}^Tk_BT & \mathbf{1} & i\mathbf{k}^T(k_BT)^2\\ 0 & i\mathbf{k}(k_BT)^2 & 0\end{pmatrix}. \tag{16}$$

From Eq. (10) we may explicitly compute the expressions for the random forces to obtain,

$$f_\mathbf{k}^\rho(t)=i\mathbf{k}\cdot\sum_i[\mathbf{x}_i(t+1)-\mathbf{x}_i(t)-\mathbf{v}_i(t)]+o(\mathbf{k}), \tag{17}$$

$$f_\mathbf{k}^{\boldsymbol{\mu}}(t)=\sum_i\left(\mathbf{v}_i(t)[i\mathbf{k}\cdot\Delta\boldsymbol{\xi}_i(t)]-\frac{1}{d}i\mathbf{k}v_i(t)^2\right)+o(\mathbf{k}), \tag{18}$$

$$f_\mathbf{k}^\varepsilon(t)=i\mathbf{k}\cdot\sum_i\left[\Delta\boldsymbol{\xi}_i(t)\left(\frac{1}{2}v_i(t)^2-C_vT\right) -\mathbf{v}_i(t)(C_p-C_v)T\right]+o(\mathbf{k}), \tag{19}$$

where we introduced the notation $\Delta\boldsymbol{\xi}_i(t)=\boldsymbol{\xi}_i(t+1)-\boldsymbol{\xi}_i(t)$. It is convenient to rewrite the momentum force as a sum of two terms; a term parallel to $\mathbf{k}$ and a perpendicular term which defines the shear viscosity coefficient,

$$f_\mathbf{k}^{\boldsymbol{\mu}}(t)=\sum_i\left(\mathbf{v}_i^\perp(t)i\mathbf{k}\cdot\Delta\boldsymbol{\xi}_i^\perp(t) +i\mathbf{k}\left[\mathbf{v}_i^\parallel(t)\Delta\boldsymbol{\xi}_i^\parallel(t)-\frac{1}{d}v_i(t)^2\right]\right)+o(\mathbf{k}),$$

where $\mathbf{v}_i^\parallel$ and $\mathbf{v}_i^\perp$ are the parallel and perpendicular components of the velocity, respectively.

Algebraic manipulations yield the following linearized hydrodynamic equations:

$$\partial_t\rho_\mathbf{k}=i\mathbf{k}\cdot\boldsymbol{\mu}_\mathbf{k}, \tag{20}$$

$$\partial_t\boldsymbol{\mu}_\mathbf{k}=i\mathbf{k}\cdot\left[k_BT\rho_\mathbf{k}+\frac{s_\mathbf{k}}{c_v}\right]+\eta\left[\mathbf{k}\mathbf{k}-\frac{1}{d}k^2\mathbf{1}\right]:\frac{\boldsymbol{\mu}_\mathbf{k}}{\rho}+\kappa\mathbf{k}\mathbf{k}:\frac{\boldsymbol{\mu}_\mathbf{k}}{\rho}, \tag{21}$$

$$\partial_ts_\mathbf{k}=k_BTi\mathbf{k}\cdot\boldsymbol{\mu}_\mathbf{k}+\lambda k^2\frac{s_\mathbf{k}}{\rho}. \tag{22}$$

The viscosity coefficient is obtained from the autocorrelation of the transverse component of $f_\mathbf{k}^{\boldsymbol{\mu}}(t)$:

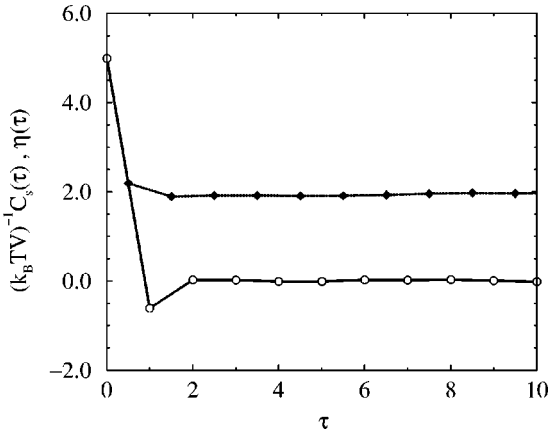

FIG. 1. The stress autocorrelation function and its running integral. The circles on the solid line show computed values of $\psi(t)$, the stress autocorrelation function. The closed diamonds on the dotted line represent the values of the partial summation of the autocorrelation function. The system size is $32\times32\times32$ and the parameter values are $\rho=10.0$ and $k_BT=\frac{1}{3}$. Rotations by $\pi/2$ in random directions were used in the collision operator.

$$\eta=\lim_{\mathsf{T}\to\infty}\frac{\rho}{2k_BTN\mathsf{T}}\sum_{t,t'<\mathsf{T}}\sum_{i,j}v_{xi}(t)\Delta\xi_{yi}(t)v_{xj}(t')\Delta\xi_{yj}(t'). \tag{23}$$

The bulk viscosity κ and heat conductivity λ transport coefficients are given by the following relations:

$$\kappa=\lim_{\mathsf{T}\to\infty}\frac{\rho}{2k_BTN\mathsf{T}}\sum_{t,t'<\mathsf{T}}\sum_{i,j}\left[\mathbf{v}_i^{\parallel}(t)\Delta\boldsymbol{\xi}_i^{\parallel}(t)-\frac{1}{d}v_i(t)^2\right]\times\left[\mathbf{v}_j^{\parallel}(t')\Delta\boldsymbol{\xi}_j^{\parallel}(t')-\frac{1}{d}v_j(t')^2\right], \tag{24}$$

$$\lambda=\lim_{\mathsf{T}\to\infty}\frac{\rho}{4C_vk_BT^2N\mathsf{T}}\sum_{t,t'<\mathsf{T}}f_{\mathbf{k}}^{\varepsilon}(t)f_{\mathbf{k}}^{\varepsilon}(t'). \tag{25}$$

C. Solvent viscosity and stress autocorrelations

The solvent viscosity and the stress autocorrelation functions are two especially important solvent properties that influence the nature of solute dynamics. We now compute these quantities by direct numerical simulation of the mesoscopic solvent model and show how simple analytical approximate values for these quantities may be obtained.

In Fig. 1 we present the results of numerical simulations of the stress–stress autocorrelation function and shear viscosity. A scattering rule was used where the velocity was rotated by $\pi/2$ in random directions. The simulations were carried out on a three-dimensional system of size $32\times32\times32$ lattice cells. Figure 1 shows both the stress–stress autocorrelation function and its time integral, whose asymptotic value is the solvent viscosity. We note that the stress autocorrelation decays to zero in about two discrete time units, setting the time scale for solvent relaxation.

Under the assumption that the stress autocorrelation function decays in a geometrical progression with rate r_η, from Eq. (23) we may derive an expression for the viscosity coefficient,

$$\eta=\lim_{\mathsf{T}\to\infty}\frac{\rho}{k_BTN}\frac{1}{2\mathsf{T}}\left(\mathsf{T}\psi(0)+\sum_{t=1}^{\mathsf{T}}2(\mathsf{T}-t)\psi(t)\right)=\rho k_BT\frac{1+r_\eta}{2(1-r_\eta)}, \tag{26}$$

where we have introduced the notation

$$\psi(t)=\left\langle\sum_{i,j}v_{xi}(t)\Delta\xi_{yi}(t)v_{xj}(t')\Delta\xi_{yj}(t')\right\rangle$$

and

$$r_\eta=\psi(1)/\psi(0).$$

If we further assume that only particles at different nodes are uncorrelated and replace $\Delta\xi_{yi}(t)$ by its expectation value $v_{yi}(t)$ we may write $\psi(1)$ as

$$\psi(1)=N\int d\mathbf{v}\,v_yv_x\overline{\mathcal{C}}_1(\overline{f}_0v_yv_x). \tag{27}$$

The operator $\overline{\mathcal{C}}_1$ is defined as

$$\overline{\mathcal{C}}_1(\overline{f}_0h_1)(\mathbf{v})=\sum_{\omega\in\Omega,n=1}^{\infty}\frac{\rho^n}{|\Omega|n!}e^{-\rho}\int d\mathbf{V}[(n)]\times\sum_{j=1}^{n}\delta(\mathbf{v}-\mathbf{v}_j)P_{\mathrm{m}}(\mathbf{V}[(n)])\sum_{i=1}^{n}h_1(\breve{\mathbf{v}}_i), \tag{28}$$

where $\breve{\mathbf{v}}_i=\mathsf{V}+\hat{\omega}[\mathbf{v}_i-\mathsf{V}]$ and $P_{\mathrm{m}}(\mathbf{V}[(n)])$ is the product of n single-particle Maxwell distributions. Computation of $\psi(0)$ from the equilibrium average yields

$$\psi(0)=N(k_BT)^2.$$

The resulting value for the viscosity coefficient is

$$\eta=\frac{\rho k_BT}{6}\frac{3(1-e^{-\rho})+2\rho}{(e^{-\rho}-(1-\rho))}. \tag{29}$$

The simulation value is $\eta=1.97$ while Eq. (29) yields $\eta=1.42$. The deviation is due to the strong correlations between colliding particles at the temperature $k_BT=1/3$.

For completeness we also give the results for the thermal conductivity. The thermal conductivity coefficient can be computed in the same way yielding

$$\lambda=\rho k_BT\frac{1+r_\lambda}{1-r_\lambda}, \tag{30}$$

with the following expression for the thermal conductivity damping constant:

$$r_\lambda=\int d\mathbf{v}s_2\overline{\mathcal{C}}_1(\overline{f}_0s_2)\Big/\int d\mathbf{v}(s_2)^2\overline{f}_0=\sum_{n=1}^{\infty}\frac{e^{-\rho}\rho^{n-1}}{15nn!}(5n^2+6n+4), \tag{31}$$

or, after summation,

$$r_\lambda=\frac{1}{15}\frac{6(1-e^{-\rho})+5\rho}{\rho}+\frac{4e^{-\rho}}{15\rho}(\mathrm{Ei}(\rho)-\gamma-\ln\rho), \tag{32}$$

where γ is Euler's constant and Ei is the exponential integral. The quantity s_2 is defined as

$$s_2=\left[\frac{c^2}{2T}-C_p\right]c_\alpha,$$

with $\mathbf{c}=\mathbf{v}-\mathbf{u}_b$, where $\mathbf{u}_b$ is the mean velocity of the solvent molecules. For the particle density used in simulations $\rho=10$ we find $r_\lambda=0.38$ and the corresponding thermal conductivity coefficient $\lambda=7.6$.

IV. BROWNIAN MOTION

In this section we illustrate the use of the hybrid MD method on the study of the diffusion of a single nanocolloidal particle and a dense nanoparticle suspension in the mesoscale solvent. For a large colloidal particle, the friction may be computed by assuming that the solvent is a viscous continuum which couples to the Brownian particle through boundary conditions. The friction coefficient ζ is given by its hydrodynamic value ζ_h, $\zeta_h=6\pi\eta R$ or $\zeta_h=4\pi\eta R$, for stick or slip boundary conditions, respectively, with R the radius of the particle.[7] In the classical theory of Brownian motion the velocity of the Brownian particle evolves by the Langevin equation[1] (we let $\mathbf{v}_{N+1}=\mathbf{u}$ to distinguish the Brownian particle velocity),

$$m_s\frac{d\mathbf{u}(t)}{dt}=-\zeta\mathbf{u}(t)+\mathbf{R}(t), \tag{33}$$

where m_s is the mass of the Brownian particle. The random force $\mathbf{R}(t)$ is assumed to be a Gaussian random process with white noise spectrum and is related to the friction by the fluctuation-dissipation theorem, $2k_BT\zeta\delta(t-t')=\langle\mathbf{R}(t)\cdot\mathbf{R}(t')\rangle/3$. The velocity correlation function, $C_u(t)=\langle\mathbf{u}(t)\cdot\mathbf{u}(0)\rangle/3$ may be computed from the Langevin equation. It decays exponentially, $C_u(t)=(k_BT/m_s)\exp(-\zeta t/m_s)$ and its infinite time integral, the diffusion coefficient, is given by the Einstein formula: $D=k_BT/\zeta$.[8]

The diffusion coefficient of a single small solute molecule possesses both microscopic and hydrodynamic components.[9] The microscopic component arises from uncorrelated collisions between the solute particle and solvent determined by the solute–solvent intermolecular forces. The hydrodynamic component is the result of hydrodynamic flows that develop around a moving particle and influence its motion. To account for the dynamics of these interactions, one may introduce a generalized Langevin equation with a time-dependent friction kernel,[8]

$$m_s\frac{d\mathbf{u}(t)}{dt}=-\int_0^t\zeta(t')\mathbf{u}(t-t')dt'+\mathbf{R}(t), \tag{34}$$

where the random force autocorrelations are related to the time-dependent friction by $2k_BT\zeta(t)=\langle\mathbf{R}(t)\cdot\mathbf{R}\rangle/3$.

A. Simulation algorithm

We consider the diffusion of large, but not macroscopically large, solute particles that interact with the solvent through continuous intermolecular forces. Using terminology introduced earlier[10] we refer to such particles as nanocolloidal particles. Since the solute particles are not macroscopically large one expects that both microscopic and hydrodynamic contributions will play a role in determining the character of the dynamics.

The system Hamiltonian is

$$\mathcal{H}=\sum_i\frac{1}{2}m_i\mathbf{v}_i^2+\sum_{i<j}V_{ij}(|\mathbf{x}_i-\mathbf{x}_j|), \tag{35}$$

where the solute particle interactions are given by truncated Lennard-Jones (LJ) potentials,

$$V(r)=\begin{cases}4\epsilon\left[\dfrac{\sigma^{12}}{r^{12}}-\dfrac{\sigma^6}{r^6}+\dfrac{1}{4}\right], & r<2^{1/6}\sigma\\ 0, & r>2^{1/6}\sigma.\end{cases} \tag{36}$$

The solute–solute interaction parameters are $\sigma_c=6.0$ and $\epsilon_c=1.0$ and the corresponding values for the solvent–solute interactions are $\sigma=3.0$ and $\epsilon=1.0$.

The dynamics of colloidal and nanocolloidal systems is characterized by a separation between the time scales that determine microscopic relaxation processes and hydrodynamic flows. The hybrid MD algorithm exploits this time-scale separation and partitions the dynamics into MD and multiparticle solvent collision steps applied consecutively to the system. During the MD step the system evolves according to Newton's equation of motion. We have used the velocity Verlet algorithm,[11]

$$\begin{aligned}\mathbf{x}_i(t+\Delta t)&=\mathbf{x}_i(t)+\Delta t\mathbf{v}_i(t)+\frac{(\Delta t)^2}{2m_i}\mathbf{F}_i(\mathbf{x}_i(t)),\\ \mathbf{v}_i(t+\Delta t)&=\mathbf{v}_i(t)+\frac{\Delta t}{2m_i}[\mathbf{F}_i(\mathbf{x}_i(t))+\mathbf{F}_i(\mathbf{x}_i(t+\Delta t))],\end{aligned} \tag{37}$$

with time step of $\Delta t=0.02\tau$ to evolve the positions and velocities in the MD step. Since solvent–solvent interactions are absent within the τ time intervals, the number of force computations needed in the full MD stages is proportional to the number of solute particles.

The time ratio $\Delta t/\tau$ is chosen based on the following considerations. The MD time step Δt is defined by the particle motion in the potential field $\Delta t\ll\sigma\sqrt{(m/k_BT)}$. The characteristic hydrodynamic time is given by the time for momentum to propagate a distance equal to the sphere radius $\tau\ll\sigma^2/\nu$, where ν is the kinematic viscosity. For the same degree of discretization error we have the following expression for the time step ratio $\Delta t/\tau\approx(\nu/\sigma)\sqrt{(m/k_BT)}=0.11$.

The interactions between solvent particles occur at each discrete time step according to the multiparticle collision dynamics using the scattering rule discussed in Sec. IV: The velocities of all solvent particles in a frame moving with the velocity of the center of mass of the particles in each cell are rotated by $\pi/2$ along a randomly chosen direction independently in each cell.

B. Heavy solute particle

We first examine the velocity autocorrelation function (VACF) and diffusion coefficient for a heavy solute particle with mass $m_s=250$ in solvent of particles with mass $m=1$, number density $\rho=10$, and $k_BT=1/3$ in the dimensionless

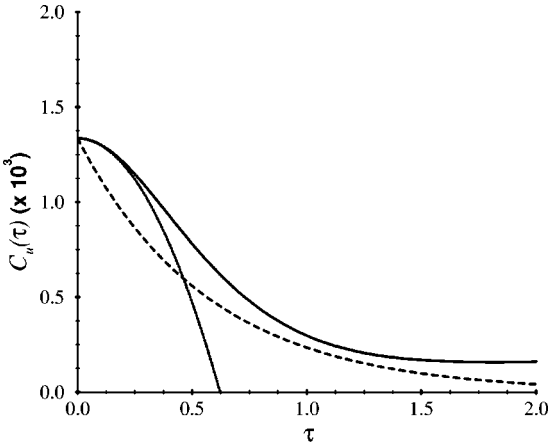

FIG. 2. Short-time behavior of the VACF for a heavy particle. The solid line shows the computed values of the VACF for particle of mass $m_s=250$ and $\sigma=3.0$. The solvent density is $\rho=10.0$ and the temperature $k_BT=\frac{1}{3}$. The excluded volume fraction of the colloidal particle is $\phi=0.02$. The dashed line shows the decay of the VACF for a hard sphere in the Boltzmann approximation. The dotted line shows the short time expansion of the VACF to second order in time calculated using the simulated value of the force autocorrelation function (see the text).

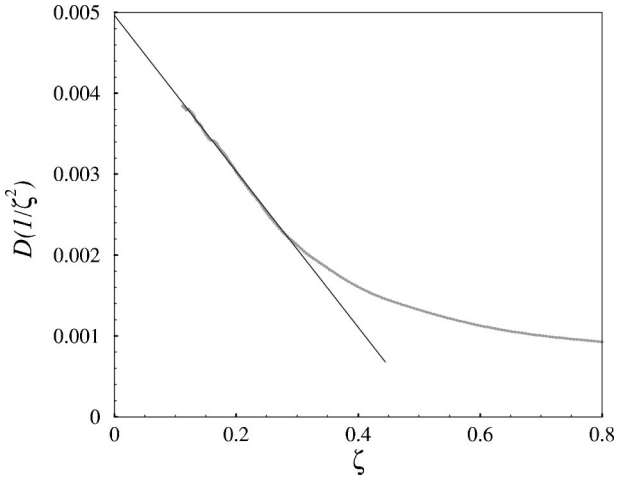

FIG. 3. The running integral of the VACF of Fig. 2 vs $\zeta=\tau^{-1/2}$. The dots show the computed values of the integral and the solid line represents a fit of the form $D(\tau)=D-\alpha_1/\sqrt{\tau}$ to the simulated values. The asymptotic value of the diffusion coefficient is $D=4.9\times10^{-3}$.

units of Sec. IV A. The mass ratio of solvent and solute particles, $r_m=m/m_s$, is $r_m=0.004$. Using σ as a rough estimate of the size of the solute particle the volume of a solute particle is $V_s=4\pi\sigma^3/3$ and the solvent–solute mass density ratio, $r_d=m\rho/(m_s/V_s)$, is $r_d=0.45$. Since both ratios are less than unity one expects relatively simple dynamics.[12]

The simulation results in Fig. 2 show the rapid short-time decay of $C_u(t)$ along with the early stages of the long-time tail. As expected for systems with continuous forces, the velocity autocorrelation function has zero initial slope. For comparison, we also show the short-time approximation to $C_u(t)$,

$$C_u(t)\sim C_u(0)-\frac{\langle F^2\rangle}{3m_s^2}\frac{t^2}{2}, \tag{38}$$

as well as the exponential decay predicted by a Boltzmann approximation to the friction coefficient, $\zeta\approx\zeta_0=(8/3)\rho\sigma^2(2\pi\mu k_BT)^{1/2}=3.5\times10^2$, where μ is the reduced mass. The corresponding diffusion coefficient equals to $D_0=k_BT/\zeta_0=1.0\times10^{-3}$. Both of these approximations fail to capture the major long-time contributions to the velocity correlation decay.

The long time behavior of running time integral of the velocity autocorrelation function gives the time-dependent diffusion coefficient,

$$D(t)=\int_0^t dt'\,C_u(t'). \tag{39}$$

Hydrodynamic contributions to the velocity autocorrelation function give rise to a $t^{-3/2}$ long time tail[13] and consequently $D(t)\approx D-\alpha_1/\sqrt{t}$. The results in Fig. 3 are in accord with this functional form, indicating the presence of a hydrodynamic component in the velocity correlation function.

If the time-dependent friction is determined from a hydrodynamic model for an incompressible fluid with either slip or stick boundary conditions one finds $\alpha_1=(2/3)\times(4\pi\eta)^{-3/2}(m_s\rho)^{1/2}$. From this expression $\alpha_1=0.0114$ while the simulation value is approximately 0.0104. The simulation and theoretical values of α_1 are in good agreement.

The existence of the $t^{-1/2}$ tail confirms that the mesoscale solvent model yields correct hydrodynamic velocity flow fields in the solvent that are responsible for this phenomenon.

The plot of $D(t)$ vs t is given in Fig. 4. The value of the diffusion coefficient determined from an extrapolation of the simulation data is $D=4.9\times10^{-3}$. If one assumes a Stokes law form with slip boundary conditions (appropriate for this system with central forces), $\zeta_h=4\pi\eta R$, and takes for the diffusion coefficient the following expression:

$$D=D_0+D_h, \tag{40}$$

one finds $R_h=3.4$, providing an estimate of the size of the microscopic boundary layer around the solute particle. We

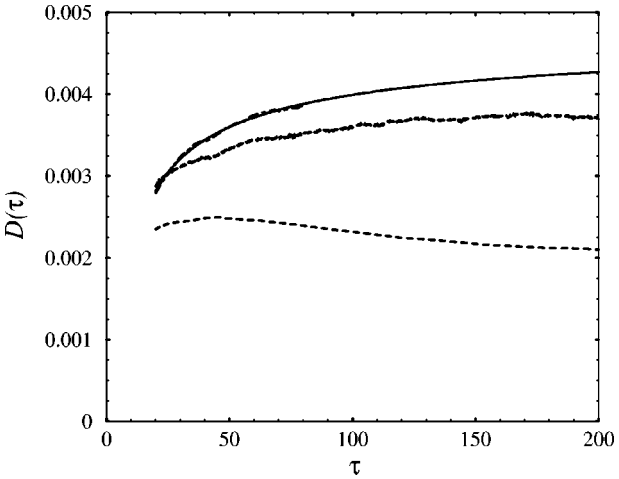

FIG. 4. The partial integrals of the VACFs for (from top to bottom) heavy particle $m_s=250$, light particle $m_s=20$ and 20 heavy particles of mass $m_s=250$ are plotted vs time.

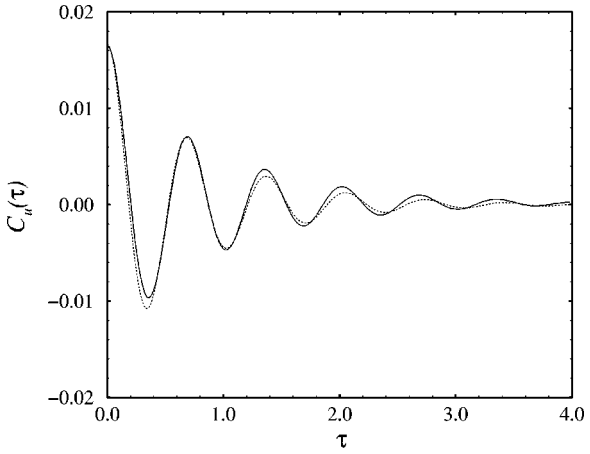

FIG. 5. Short-time behavior of the VACF for a particle of mass $m_s=20$. The other parameters are the same as in Fig. 2. The solid and the dotted lines show the simulation values of VACF and the values computed from an exponentially decaying memory function approximation, respectively.

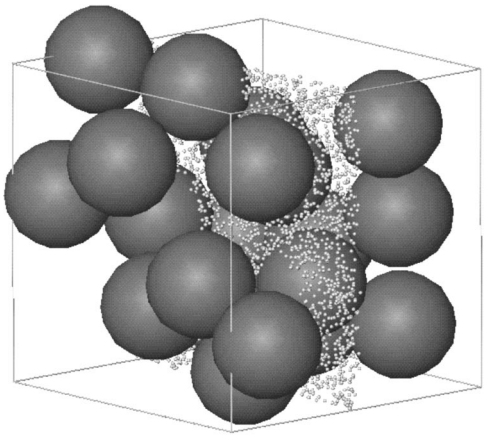

FIG. 6. A snapshot of a configuration of solute and solvent molecules. Large particle radii are $r=2^{1/6}\sigma$. Solvent particles in a rectangular slab with coordinates $9.5<x<10.5$ are drawn as light small balls. The excluded volume fraction for the system is $\phi=0.4$. Due to periodic boundary conditions some large particles are seen outside the system borders marked by the light wire frame.

note that as we compute D by extrapolating the stress autocorrelation function we do not need to take into account the negative finite size correction $\sim\sigma/L$, which is a result of momentum conservation in finite volume simulations. The finite size correction gives a significant contribution to the value of the diffusion coefficient.[14]

C. Caging effects for a light solute particle

We next consider a solute particle of mass $m_s=20$ in the same solvent so that $r_m=0.05$ and $r_d=5.56$. Thus, while the solute particle mass is large its mass density is not and one expects more complex dynamics.[12] Figure 5 shows the velocity autocorrelation function and one observes strong oscillations as a result of the caging of the solute particle by the solvent. A simple model may be constructed for these oscillations. Consider the expression for the half-sided Fourier transform of the velocity autocorrelation function obtained from the generalized Langevin equation. Multiplying Eq. (34) by $\mathbf{u}(0)$ and taking the Fourier transform of both sides we arrive, after averaging, at the following expression:

$$\tilde{C}_u(\omega)=\frac{k_BT}{-m_s i\omega+\tilde{\zeta}(\omega)}. \tag{41}$$

We expect that at short times the solute particle experiences uncorrelated collisions with the solvent particles which are exponentially distributed in time. We may then assume that the friction coefficient $\zeta(t)$ decays exponentially for short times,

$$\zeta(t)=m_s\omega_f^2 e^{-\omega_\zeta t}, \tag{42}$$

where ω_f is defined by the force–force autocorrelation $\omega_f^2=\langle F_x^2\rangle/(m_sk_BT)$.

Using the Fourier transform of this time-dependent friction coefficient in Eq. (41) and inverting the transform to obtain the velocity autocorrelation function, we obtain

$$C_u(t)=\frac{k_BT}{m_s}e^{-\omega_\zeta t/2}\left(\cos\omega_0 t+\frac{\omega_\zeta}{2\omega_0}\sin\omega_0 t\right), \tag{43}$$

where $\omega_0^2=\omega_f^2-\omega_\zeta^2/4$. In Fig. 5 we compare the short-time autocorrelation function obtained in simulations (solid line) with a fit to Eq. (43) (dotted line). The parameters of the fit are $\omega_\zeta=2.59$ and $\omega_0=9.20$. (A single parameter enters the fit since ω_0 may be determined from ω_f and ω_ζ.) This expression captures the main features of the short-time oscillations.

The collision contribution to the diffusion coefficient arising from this effect is given by $D_0=\tilde{C}_u(0)$,

$$D_0=\frac{k_BT\omega_\zeta}{m_s\omega_f^2}. \tag{44}$$

The theoretical value of the collision contribution to the value of the diffusion coefficient given by Eq. (44) is $D_0=5.0\times10^{-4}$ and constitutes a few percent of the total diffusion coefficient, $D=3.6\times10^{-3}$, which can be determined from the simulation results in Fig. 4. Again assuming a Stokes law friction we find $R_h=4.3$, indicating larger microscopic boundary layer effects in this light mass density case.

D. Concentrated nanocolloidal suspensions

To study self-diffusion in concentrated colloidal suspensions one must account for solute–solute interactions arising from the direct intermolecular potentials as well as hydrodynamic interactions due to the perturbation of the flow fields by other solute molecules. The Langevin equation must now be replaced by a coupled set of Langevin equations for the velocities of all the solute molecules. The volume fraction dependence of the self-diffusion coefficient in concentrated suspensions has been studied extensively, both theoretically[15–19] and experimentally.[20]

We have carried out a simulation of the dynamics of 20 solute particles of mass $m_s=250$ in the mesoscale solvent with the same density and temperature as in the single particle cases treated previously. The volume fraction is $\phi=0.4$. In Fig. 6 we show a configuration of the solute particles in this concentrated suspension. The solvent molecules

of the mesoscale solvent model are shown in a thin slice through the three-dimensional volume in order to avoid obscuring the solute particles. From Fig. 6 one can see that the interactions governing the motion of a tagged solute particle will involve both solute-solute interactions and the above-described complex many-body hydrodynamic interactions.

The time-dependent diffusion coefficient $D(t)$ obtained from the running integral of the velocity correlation function is shown in Fig. 4. One can see that the diffusion coefficient is smaller than that for a single solute particle of the same size and mass. In addition, $D(t)$ increases rapidly to a broad maximum and then falls slowly on a long time scale before reaching its asymptotic value.

A quantity that can be measured in experiments is the short-time self-diffusion coefficient, D_s. This diffusion coefficient describes the dynamics on time scales t such that $\tau_H \ll t \ll \tau_D$, where τ_H is the hydrodynamic screening time within which hydrodynamic interactions become important and τ_D is structural relaxation time of the suspension.[19] For the system considered here $\tau_H \approx 30$ while $\tau_D \approx 1000$. The coefficient D_s reflects the decay of the velocity autocorrelation function that occurs on time scales that are sufficiently short that the solute particle configuration does not change appreciably. The short-time diffusion coefficient can be extracted from the broad maximum of $D(t)$ in Fig. 4. From the data presented in Fig. 4 one may estimate the ratio $D_s/D \approx 0.5$, where D is the diffusion coefficient for a single solute particle. While there are no theoretical estimates for this ratio for the Lennard-Jones system we study, we note that the theoretical estimates for hard-sphere suspensions yield $D_s/D \approx 0.32$ for a volume fraction of $\phi = 0.4$.[19]

For long times the configuration of solute particles changes and dynamical effects arising from a variety of solute–solute interactions come into play leading to a decrease in the diffusion coefficient.

V. CONCLUSION

When constructing hybrid MD schemes which treat solvent motions on a mesoscale level it is essential that the solvent dynamics exhibit the correct hydrodynamics on long scales, yet couples to the solute molecules in a manner that reflects specific features of solute–solvent intermolecular forces. The mesoscale solvent model constructed in Ref. 2 was shown to yield the correct hydrodynamic equations of motion and exhibit flow fields with the correct features even on small scales where its particle nature is apparent.

The hybrid MD scheme discussed in this paper exploits the particle nature of the solvent to describe the solute–solvent interactions microscopically, rather than through boundary conditions imposed at the surface of solute molecules. As a result of these two features the hybrid MD scheme can be used to model solute dynamics when specific features of solute–solvent interactions are important.

The efficiency of the scheme derives from the fact that the solvent–solvent interactions are considered only at discrete time intervals and modeled by a multiparticle collision rule that accounts for the effects of all solvent–solvent collisions in the time interval. The combination of full MD with discrete-time solvent–solvent collisions is straightforward to implement numerically but presents some theoretical features that required the more detailed considerations given in Sec. III.

The simulations of solute particle motion presented here show that both microscopic and hydrodynamic effects are captured by the hybrid MD scheme and have served to demonstrate the feasibility and utility of the method. The method should find application in more complex problems such as polymer dynamics in solution or studies of solution-phase reaction dynamics.

ACKNOWLEDGMENT

This work was supported in part by a grant from the Natural Sciences and Engineering Research Council of Canada.

APPENDIX A: EQUATIONS OF MOTION

Applying the projection operators $\mathcal{P}$ and $\mathcal{Q}$ to Eq. (5) we obtain a system of two equations,

$$\mathsf{P}_{\mathcal{P}}(t+1) = \mathcal{P}\mathcal{W}\mathsf{P}_{\mathcal{P}}(t) + \mathcal{P}(\mathcal{W}-1)\mathsf{P}_{\mathcal{Q}}(t), \tag{A1}$$

$$\mathsf{P}_{\mathcal{Q}}(t+1) = \mathcal{Q}(\mathcal{W}-1)\mathsf{P}_{\mathcal{P}}(t) + \mathcal{Q}\mathcal{W}\mathsf{P}_{\mathcal{Q}}(t), \tag{A2}$$

where $\mathsf{P}_{\mathcal{P}}(t) = \mathcal{P}\mathsf{P}(t)$ and $\mathsf{P}_{\mathcal{Q}}(t) = \mathcal{Q}\mathsf{P}(t)$. A recursive application of Eq. (A2) yields the result,

$$\mathsf{P}_{\mathcal{Q}}(t) = [\mathcal{Q}\mathcal{W}]^t \mathsf{P}_{\mathcal{Q}}(0) + \sum_{\tau=1}^{t} [\mathcal{Q}\mathcal{W}]^{\tau-1} \mathcal{Q}(\mathcal{W}-1)\mathsf{P}_{\mathcal{P}}(t-\tau), \tag{A3}$$

which, after substitution into Eq. (A1), gives

$$\mathsf{P}_{\mathcal{P}}(t+1) = \mathcal{P}\mathcal{W}\mathsf{P}_{\mathcal{P}}(t) + \sum_{\tau=1}^{t} \mathcal{K}(\tau-1)\mathsf{P}_{\mathcal{P}}(t-\tau), \tag{A4}$$

where the memory kernel is defined by

$$\mathcal{K}(\tau) = \mathcal{P}(\mathcal{W}-1)[\mathcal{Q}\mathcal{W}]^{\tau}\mathcal{Q}(\mathcal{W}-1)\mathcal{P}. \tag{A5}$$

We eliminated the first term on the right-hand side of relation (A3) by the use of a specially prepared ensemble of initial conditions where deviations only occur in the dynamical variables. For slowly decaying dynamical variables, which are our main concern, $\mathsf{P}_{\mathcal{P}}(t-\tau)$ can be replaced by $\mathsf{P}_{\mathcal{P}}(t)$.

Equations (A4) and (A5) hold for the projection onto any set of dynamical variables. Next, we consider the forms they take for conserved variables for small $\mathbf{k}$. If the dynamics given by a composition of streaming and collision in that order, the following identity holds for conserved variables:

$$\sum_i \boldsymbol{\iota}_i(t) e^{i\mathbf{k}\cdot\mathbf{x}_i(t)} = \sum_i \boldsymbol{\iota}_i(t-1) e^{i\mathbf{k}\cdot\mathbf{x}_i(t)}. \tag{A6}$$

Equation (A6) follows from the conservation of the quantities $\boldsymbol{\iota}$ under collisions at time $t+1$. Using identity (A6) and expanding $\mathbf{a}$ in powers of $\mathbf{k}$, we write the $\mathcal{P}$ projection of $[\mathcal{W}-1]b$, where b is an arbitrary function, as

$$(\mathcal{P}[\mathcal{W}-1]b)(\Gamma)=\mathbf{a}^\dagger(\Gamma)P_0(\Gamma)\langle\mathbf{a}\mathbf{a}^\dagger\rangle^{-1}\int d\Gamma'[\mathbf{a}(\mathcal{S}(\Gamma',1))-\mathbf{a}(\Gamma')]b(\Gamma') \tag{A7}$$

$$=\mathbf{a}^\dagger(\Gamma)P_0(\Gamma)\langle\mathbf{a}\mathbf{a}^\dagger\rangle^{-1}\int d\Gamma'\left[e^{i\mathbf{k}\cdot\mathbf{x}(\Gamma'/i)(t)}b(\Gamma')\sum_i (i\mathbf{k}\cdot[\mathbf{x}_i'(1)-\mathbf{x}_i'(0)]\iota_i'(0)+o(\mathbf{k}))\right]. \tag{A8}$$

Along the same lines we may prove that $[\mathcal{W}-1]\mathcal{P}=O(\mathbf{k})$.

Next, we shall prove that

$$[\mathcal{Q}\mathcal{W}]^\tau\mathcal{Q}=\mathcal{Q}\mathcal{W}^\tau\mathcal{Q}+O(\mathbf{k}). \tag{A9}$$

For $\tau=0$ relation (A9) holds. Let us assume that it holds for $\tau=l$ and prove the relation for $\tau=l+1$. We write $[\mathcal{Q}\mathcal{W}]^{l+1}\mathcal{Q}=[\mathcal{Q}\mathcal{W}]^l\mathcal{Q}\mathcal{W}\mathcal{Q}$. Then

$$\begin{aligned}[\mathcal{Q}\mathcal{W}]^{l+1}\mathcal{Q}&=[\mathcal{Q}\mathcal{W}]^l\mathcal{Q}\mathcal{W}\mathcal{Q}=\mathcal{Q}\mathcal{W}^l\mathcal{Q}\mathcal{W}\mathcal{Q}+O(\mathbf{k})\\&=\mathcal{Q}\mathcal{W}^l[\mathcal{Q}+(\mathcal{W}-1)+O(\mathbf{k})]\mathcal{Q}+O(\mathbf{k})\\&=\mathcal{Q}\mathcal{W}^{l+1}\mathcal{Q}+O(\mathbf{k}),\end{aligned} \tag{A10}$$

where we reexpressed $\mathcal{Q}\mathcal{W}$ in the equivalent form

$$\mathcal{Q}\mathcal{W}=\mathcal{Q}+(\mathcal{W}-1)-\mathcal{P}(\mathcal{W}-1)=\mathcal{Q}+(\mathcal{W}-1)+O(\mathbf{k}). \tag{A11}$$

This proves the assertion of the recursion relation and, thus, the formula (A9).

From relation (A7), its dual expression, and formula (A9) we may express the memory kernel equation as

$$\mathcal{K}(\tau)=\mathcal{P}(\mathcal{W}-1)\mathcal{Q}\mathcal{W}^\tau\mathcal{Q}(\mathcal{W}-1)\mathcal{P}+o(\mathbf{k}^2),$$

which is Eq. (8) in Sec. III.

APPENDIX B: SIMPLIFICATION OF EQUATIONS OF MOTION

In this Appendix we show how the formal equations of motion for the average values of conserved dynamical variables can be written in a convenient form. Computing the average of $\mathbf{a}$ over the projected probability distribution (7) yields the following set of equations for the average values $\overline{\mathbf{a}}(t)$:

$$\overline{\mathbf{a}}(t+1)-\overline{\mathbf{a}}(t)=\langle(\mathbf{a}(\mathcal{S}(\Gamma,1))-\mathbf{a}(\Gamma))\mathbf{a}^\dagger(\Gamma)\rangle\langle\mathbf{a}\mathbf{a}^\dagger\rangle^{-1}\overline{\mathbf{a}}(t)+\sum_{\tau=1}^{t}\langle\mathbf{a}(\mathcal{W}-1)\mathcal{Q}\mathcal{W}^{\tau-1}\mathcal{Q}(\mathcal{W}-1)\mathbf{a}^\dagger\rangle\langle\mathbf{a}\mathbf{a}^\dagger\rangle^{-1}\overline{\mathbf{a}}(t-\tau). \tag{B1}$$

We rewrite the first term on the right-hand side of Eq. (B1) as a sum of symmetric and antisymmetric operators:

$$\langle(\mathbf{a}(\mathcal{S}(\Gamma,1))-\mathbf{a}(\Gamma))\mathbf{a}^\dagger(\Gamma)\rangle=\tfrac{1}{2}\langle\mathbf{a}(\mathcal{S}(\Gamma,1))\mathbf{a}^\dagger(\Gamma)-\mathbf{a}(\Gamma)\mathbf{a}^\dagger(\mathcal{S}(\Gamma,1))\rangle-\tfrac{1}{2}\langle(\mathbf{a}(\mathcal{S}(\Gamma,1))-\mathbf{a}(\Gamma))(\mathbf{a}^\dagger(\mathcal{S}(\Gamma,1))-\mathbf{a}^\dagger(\Gamma))\rangle, \tag{B2}$$

where we used time-translation invariance of the equilibrium probability distribution,

$$\langle\mathbf{a}(\mathcal{S}(\Gamma,1))\mathbf{a}^\dagger(\mathcal{S}(\Gamma,1))\rangle=\langle\mathbf{a}(\Gamma)\mathbf{a}^\dagger(\Gamma)\rangle.$$

For the memory kernel acting on $\langle\mathbf{a}\mathbf{a}^\dagger\rangle^{-1}\overline{\mathbf{a}}$ we write

$$\langle\mathbf{a}(\mathcal{W}-1)\mathcal{Q}\mathcal{W}^{t-1}\mathcal{Q}(\mathcal{W}-1)\mathbf{a}^\dagger\rangle=\langle\mathbf{f}(t)\mathbf{f}^\dagger(0)\rangle, \tag{B3}$$

with

$$\begin{aligned}\mathbf{f}(t)=&\mathbf{a}(\mathcal{S}(\Gamma,t+1))-\langle\mathbf{a}(\mathcal{S}(\Gamma',1))\mathbf{a}^\dagger(\Gamma')\rangle\\&\times\langle\mathbf{a}\mathbf{a}^\dagger\rangle^{-1}\mathbf{a}(\mathcal{S}(\Gamma,t)),\end{aligned} \tag{B4}$$

where we used the time-translation invariance of equilibrium averages.

Letting $\mathbf{b}(\Gamma)=\mathbf{a}(\mathcal{S}(\Gamma,1))-\mathbf{a}(\Gamma)$, we write the second term of Eq. (B2) as

$$\tfrac{1}{2}\langle\mathbf{b}(\Gamma)\mathbf{b}^\dagger(\Gamma)\rangle=\tfrac{1}{2}\langle\mathbf{b}(\Gamma)\mathcal{Q}\mathbf{b}^\dagger(\Gamma)\rangle+\tfrac{1}{2}\langle\mathbf{b}(\Gamma)\mathcal{P}\mathbf{b}^\dagger(\Gamma)\rangle. \tag{B5}$$

First, we notice that $\mathcal{Q}\mathbf{b}^\dagger(\Gamma)=\mathbf{f}^\dagger(0)$ and, thus, the first term has the same form as the summands of the memory kernel: $\langle\frac{1}{2}\mathbf{f}\mathbf{f}^\dagger\rangle$. The second term in Eq. (B5) may be expressed as

$$\begin{aligned}\langle\mathbf{b}(\Gamma)\mathcal{P}\mathbf{b}^\dagger(\Gamma)\rangle=&-\langle(\mathbf{a}(\mathcal{S}(\Gamma,1))-\mathbf{a}(\Gamma))\mathbf{a}^\dagger(\Gamma)\rangle\\&\times\langle\mathbf{a}\mathbf{a}^\dagger\rangle^{-1}\langle\mathbf{a}(\Gamma)(\mathbf{a}^\dagger(\mathcal{S}(\Gamma,1))-\mathbf{a}^\dagger(\Gamma))\rangle.\end{aligned}$$

Furthermore, we may show that

$$\begin{aligned}&[\tfrac{1}{2}\langle\mathbf{a}(\mathcal{S}(\Gamma,1))\mathbf{a}^\dagger(\Gamma)-\mathbf{a}(\Gamma)\mathbf{a}^\dagger(\mathcal{S}(\Gamma,1))\rangle\langle\mathbf{a}\mathbf{a}^\dagger\rangle^{-1}]^2\\&\quad=-\langle\mathbf{b}(\Gamma)\mathcal{P}\mathbf{b}^\dagger(\Gamma)\rangle\langle\mathbf{a}\mathbf{a}^\dagger\rangle^{-1}+o(\mathbf{k}^2).\end{aligned}$$

Indeed,

$$\begin{aligned}&\tfrac{1}{2}\langle\mathbf{a}(\mathcal{S}(\Gamma,1))\mathbf{a}^\dagger(\Gamma)-\mathbf{a}(\Gamma)\mathbf{a}^\dagger(\mathcal{S}(\Gamma,1))\rangle\\&\quad-\langle(\mathbf{a}(\mathcal{S}(\Gamma,1))-\mathbf{a}^\dagger(\Gamma))\mathbf{a}(\Gamma)\rangle\\&\quad=\tfrac{1}{2}\langle[\mathbf{a}(\Gamma)-\mathbf{a}(\mathcal{S}(\Gamma,1))][\mathbf{a}^\dagger(\Gamma)-\mathbf{a}^\dagger(\mathcal{S}(\Gamma,1))]\rangle=o(\mathbf{k}),\end{aligned}$$

with a similar expression for the second factor.

Next, we consider some general aspects of discrete-time dynamics. Suppose that the time evolution of the system is given by the following Euler scheme:

$$\overline{a}(t+1)=\overline{a}(t)+[\mathcal{A}-\mathcal{B}]\overline{a}(t),$$

where $\mathcal{A}$ and $\mathcal{B}$ are of the first and second orders in $\mathbf{k}$. In this case we write the operator identity

$$\exp\left(\frac{\partial}{\partial t}\right) = 1 + \mathcal{A} - \mathcal{B},$$

or, by expanding the logarithm into a Taylor series up to second order in **k** we obtain

$$\frac{\partial}{\partial t} = \mathcal{A} - \frac{1}{2}\mathcal{A}^2 - \mathcal{B}. \tag{B6}$$

Combining Eqs. (B6), (B5), (B2), and (B3) we find Eq. (9) of Sec. III.

[1] S. Chandrasekhar, Rev. Mod. Phys. **15**, 1 (1943;).
[2] A. Malevanets and R. Kapral, J. Chem. Phys. **110**, 8605 (1999).
[3] G. A. Bird, *Molecular Gas Dynamics* (Clarendon, Oxford, 1976); G. A. Bird, Comput. Math. Appl. **35**, 1 (1998).
[4] Related derivations have been carried out in Jean-Pierre Rivet, Complex Syst. **1**, 839 (1987); M. H. Ernst, in *Microscopic Simulations of Complex Hydrodynamics Phenomena*, edited by M. Mareschal and B. Holian (Plenum, New York, 1992), p. 153.
[5] R. Zwanzig, J. Chem. Phys. **33**, 1338 (1960).
[6] H. Mori, Prog. Theor. Phys. **33**, 423 (1965).
[7] L. D. Landau and E. M. Lifshitz, *Fluid Mechanics* (Pergamon, New York, 1959).
[8] R. Kubo, in *Many-body Problems*, edited by W. E. Parry (W. A. Benjamin, New York, 1969).
[9] J. T. Hynes, R. Kapral, and M. Weinberg, J. Chem. Phys. **70**, 1456 (1979).
[10] M. J. Nuevo, J. J. Morales, and D. Heyes, Phys. Rev. E **58**, 5845 (1998).
[11] W. C. Swope, H. C. Andersen, P. H. Berens, and K. R. Wilson, J. Chem. Phys. **76**, 673 (1982); M. Tuckerman, B. J. Berne, and G. J. Martyna, *ibid.* **97**, 1990 (1992).
[12] M. Tokuyama and I. Oppenheim, Physica A **94**, 501 (1978).
[13] B. J. Alder and T. E. Wainwright, Phys. Rev. Lett. **18**, 988 (1967).
[14] B. Dunweg and K. Kremer, Phys. Rev. Lett. **66**, 2996 (1991).
[15] C. W. J. Beenakker and P. Mazur, Physica A **120**, 388 (1983).
[16] G. K. Batchelor, J. Fluid Mech. **74**, 1 (1965).
[17] B. J. Felderhof, J. Phys. A **11**, 929 (1978).
[18] R. B. Jones, Physica A **97**, 113 (1979).
[19] M. Tokuyama and I. Oppenheim, Physica A **216**, 85 (1995).
[20] P. N. Pusey and W. van Megen, Nature (London) **320**, 340 (1986); *Dynamic Light Scattering*, edited by R. Pecora (Plenum, New York, 1985); W. Van Megan, I. Snook, and P. N. Pusey, J. Chem. Phys. **78**, 931 (1983).